

Experimental and Numerical Analysis of the Polyvinyl Chloride (PVC) Mechanical Behavior Response

H. Khellafi¹, H.M. Meddah¹, B. Ould Chikh¹, B. Bouchouicha²,
M. Benguediab², M. Bendouba³

Abstract: The polyvinyl chloride PVC is a polymer material widely used for a large variety of applications. The present work focuses on the identification of the physical processes responsible for the mechanical properties of the PVC containing different crystallinities rate applied in large deformation and different strain rates. In order to understand the behavior of the PVC, a thermodynamic modeling is needed. Therefore, the contribution of this approach was demonstrated by experiment and numerical modeling. This comparative study demonstrates that the proposed model provides better agreement with experimental evidence.

Keywords: Damage; Fracture; PVC; Numerical analysis; FEM.

1 Introduction

The polymers are inseparable from our environment and our practical life. They have established themselves in all areas of our business through their use in hygiene and food products. Most often synthetic, sometimes natural, they must rise to their wide range of features, hard, soft and elastic, transparent or opaque, insulated and occasionally conductors, more or less resistant to aggressive conditions of their use, always lightweight. The semi-crystalline polymers are materials that having a complicated microstructure consisted of an amorphous disordered phase and a vicious nature structured crystalline phase. Coexistence and interaction of these two phases of very different natures are the origin of the complexity of their macroscopic behavior that could fall within the scope of such as elasto-viscoplastic behavior [Kichenin (1992); Paquin and Berveiller (1996); Ouakka, Dang Van, Gueugnaut, and Blouet (1997); Polanco-Loria, Clausen, Berstad, and Hopperstad (2007)]. Several fracture study ways were investigated, the first take place on the scale of the

¹ LSTE Laboratory, University of Mascara, BP 763 Mascara, Algeria

² LMSR Laboratory, University of Sidi Bel Abbes, Algeria

³ LPQ3M Laboratory, University of Mascara, BP 763, Mascara, Algeria

continuum mechanics. This approach allows predicting the evolution of this latter according to the state of loading and leads to a characterization of mechanical quantities at the instant of the rupture. Other phenomenological approaches are looking for simple mathematical models in order to translate sufficient conditions for the rupture is primed.

The expression of criteria and descriptors put into play may be different according to the importance of the plastic process developing in the material. The polymers are composed of macromolecules that are obtained by adding small molecules called monomers. When a polymerization reaction is happened, the monomers are generally of long chains that can fold on themselves and/or entangle with neighboring macromolecules. The long chain polymer can have crystalline domains and/or amorphous as appropriate. Our aim is to depict the different routes of possible study and choose the most appropriate to the description of our material (PVC), establishing laws of behavior of Gurson Model [Gurson (1977)] and rupture criteria relevant implementable in a numerical simulation of the behavior of the PVC structure commonly used in the industry. We firstly present present much information that will glimpse the importance of the combined effects of the formulation and implementation of PVC.

2 Analytical modeling of the strain rate deformation of polymers

Modeling of polymers is based initially on the rheological model of Voigt and Maxwell. These models are used to combine both of viscoelastic and Viscoplasticity [Lamloumi, Hassini, Lecomte-Nana, Elcafsi, and Smith (2014)], two behaviors encountered in polymers. In the case of semi-crystalline, although the behavior of the amorphous phase is very different from the behavior of the crystalline phase, many models have tried to describe by means of a unique equation of the two-phase behavior [Gurson (1977)] Other models, based on the Eyring equation [Bahadur (1977)] make it possible to account for the rubber elasticity of the amorphous phase as well as the deformation of the crystalline phase [Eyring (1936)]. Other models have chosen to rely solely on modeling the crystalline texture [G'sell and Jonas (1981)]. The polymer is then considered as a polycrystalline aggregate of crystallites formed randomly. The crystalline phase is believed to have a viscoelastic behavior, crystalline lamellae deforming sliding, parallel or perpendicular to the channels. The failure to take into account the contribution of the amorphous phase to plastic deformation implies an underestimation of the plastic hardening, especially in shear. This will be checked especially as the amount of amorphous phase is important in the polymer. To take into account the contribution of the amorphous phase, the previous model is complemented by the model Van Der Giessen dealing with the rubber elasticity [Dahoun (1992)]. This model adds two param-

eters: density in the crystallises and limited by the average number of segments by sub channels flexible chains. To combine the two models, the mean stress is decomposed due to the stress between the crystalline phase and the stress due to the amorphous phase such as (1):

$$\bar{\sigma} = X_c \sigma^c + (1 - X_c) \sigma^a \quad (1)$$

X_c : Is a constant in eq (1).

The introduction of Van Der Giessen model [Wu and Van Der Giessen (1993)] to account for the contribution of the amorphous phase improves the original Dahoun model [Dahoun (1992)]. However, the juxtaposition of both models as shown in the equation above is nevertheless a simplification since no coupling or interaction between the two phases are taken into account. It is seen that the complexity of the semi-crystalline structures seriously complicates models compared to amorphous polymers, formed from a single homogeneous phase behavior. Modeling of these is then often taken as a basis for reflection.

2.1 The criterion of gurson

In connection with the approach mentioned above, the model comprises a Gurson flow condition, a measure of the volume fraction of voids, a law characteristic nucleation and a law of evolution cavities. This volume increases in polymers due to void growth is commonly reported in many recent studies [G'sell and Dahoun (1994); Laiarinandrasana, Morgeneyer, Proudhon, N'guyen, and Maire (2012)].

The flow function has been obtained in the following manner:

- The Von Mises criterion is used to characterize the flow of the matrix.
- A rigid plastic model is assumed to be valid due to its large deformation caused by the process of ductile fracture.
- A form of the velocity field is considered in the aggregate to enable the cavities to grow while maintaining the incompressibility of the plastic matrix. This velocity field must also verify the kinematic boundary conditions of the tensor of deformation rate on the surfaces of a unit cell of cubic shape. Based on these assumptions, an approximate flow of a porous material according to which stress depends on the macroscopic, microscopic flow stress of the matrix and the volume fraction of actual cavities is obtained as follows (2):

$$\Phi(\underline{\sigma}, \sigma_0, f) = \frac{\sigma_{eq}^2}{\sigma_0^2} + 2f \cos sh\left(\frac{3}{2} \frac{\sigma_m}{\sigma_0}\right) - 1 - f^2 = 0 \quad (2)$$

With:

Φ : Function of flow

σ_{eq} : The equivalent macroscopic stress

σ_m : Average macroscopic stress

f : The porosity of the material

σ_0 : The limit of elasticity of the matrix

$\underline{\sigma}$: The macroscopic stress tensor (matrix + pores)

Gurson model gives satisfactory approximations for high triaxiality constraints but, overestimates the fracture strain of the material for low levels of triaxiality.

2.2 Mechanical behavior

Despite large differences in the nature and structure of metals (and alloys) and polymers (and composite), we paradoxically observed strong similarities in their macroscopic behavior. Thus, with orders of magnitude different, the terms of elasticity, viscosity, plastic deformation, hardening, brittle fracture, ductile failure, apply to all such materials. This is what justifies a priori the overall approach to the mechanics of materials using the concepts of continuum mechanics.

Thermodynamics and rheology, it allows building models that do not depend on their foundations of the materials. Thus, it is not uncommon for the analysis methods of the mechanical properties developed for the metals are applied to polymers. However, if the rheological behavior of materials appears to involve macroscopic phenomena similar, they differ in the basic phenomena involved as well as their magnitude. This is the case for example for the way they develop or not necking (plastic instability observed in simple tension beyond a certain critical strain). Experimentally this phenomenon, which often occurs at the center of the specimen [Castagnet and Deburek (2007); Laiarinandrasana, Besson, Lafarge, and Hochstetter (2009); Boisot, Laiarinandrasana, Besson, Fond, and Hochstetter (2011)], is characterized by a concentration of the local plastic deformation. For a metal, this local thinning is increasing more and more up to the lead to rupture of the specimen. In contrast, for some polymers, the thinning of the striation stabilizes and then we observed a propagation shoulder of the striation. The experimental test is performed to determine the behavior law of PVC; the specimen was collected in the form of a plate. Geometry corresponds to the ASTM D638 standard M1A [ASTM D638 (2010)] as shown in Fig. 1.

The test was performed on an Instron tensile testing machine at room temperature of 23°C. Different elastoplastic material properties can be obtained from the stress-

strain curve (see Fig 1.a). The mechanical properties of PVC used are presented in Tab. 1.

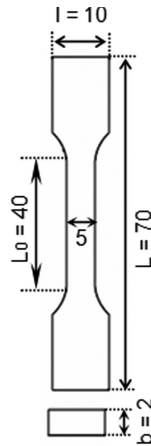


Figure 1: Specimens geometry used in tension test.

Table 1: Mechanical properties of the Polyvinyl Chloride (PVC).

$d\varepsilon/dt$ (S^{-1})	E (MPa)	σ_y (MPa)	ν	Specific gravity
0.1	656	50		
0.01	652	42	0.4	0.87
0.001	650	40		

Fig. 2. (b), (c) and (d) shows the experimental and numerical stress-strain curve for different strain rate ($\nu = 0.1$, $\nu = 0.01$ and $\nu = 0.001$). These figures show the typical response of PVC under tensile, consisting of three regions: an initial linear elastic phase, a stress plateau and a densification stage, characterized by a steep stiffness increase. Results show very good comparison between the numerical predictions obtained from the FE models and experimental data. The developed FE model using is capable of predicting with some accuracy not only the duration and peak stress of the impact at different strain rate, but also the typical nonlinear shape of the stress-strain curves. The experimental and numerical comparison showed to be in a good agreement.

2.3 Numerical study

Many recent papers in fracture analysis of complex 2D & 3D solid structures and materials are presented [see, Dong and Atluri (2012a); Dong and Atluri (2012b);

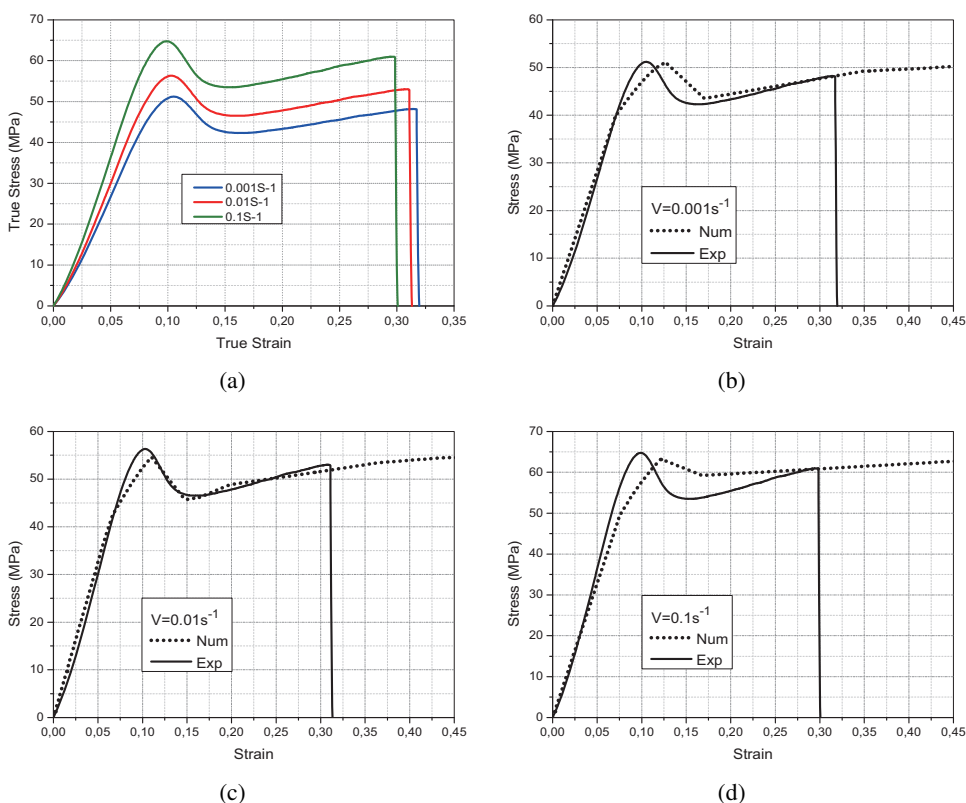


Figure 2: Stress vs Strain curves a) Experimental analysis, b) experimental and numerical cures at $V = 0.001 \text{ s}^{-1}$, c) experimental and numerical cures at $V = 0.01 \text{ s}^{-1}$, d) experimental and numerical cures at $V = 0.1 \text{ s}^{-1}$.

Bendouba, Djebli, Aid, Benseddig, and Benguediab (2015)]. Working on axisymmetric notched specimens (AE) as presented in [Meddah, Selini, Benguediab, Bouziane, and Belhamiani (2009); Ognedal, Clausen, Dahlen, and Hopperstad (2014); Ognedal, Clausen, Berstad, Seelig, and Hopperstad (2014)], it is possible to study multiaxial loading, only using a tensile test. These specimens allow overcoming stress conditions plane strain. For a notched, as the elastic limit is not exceeded the maximum constraint is on the bottom of notch phenomenon by stress concentration. The yield strength is reached first at this location. If the test continues to be deformed plastically, the deformed area expands and eventually invaded the notched section. The load reaches the limit load of the specimen. To meet the criterion of plasticity (Von Mises or Tresca), it is necessary to increase all the axial stress. Thus, plastic deformation confined raises the general level of stress and the

rate of stress triaxiality β . This is defined as (7):

$$\beta = \frac{\sigma_m}{\sigma_{eq}} \quad (3)$$

$$\sigma_m = \left(\frac{1}{3}(\sigma_{11} + \sigma_{22} + \sigma_{33})\right)$$

σ_m : The mean stress

σ_{eq} : The equivalent Von Mises stress.

For a cylindrical test piece having a groove notch root radius (R) leaving a collar of radius (a) in the minimum cross section (Figure 2), the calculation of distribution of stress and strain is complicated and not fully resolved analytically. Simplifying assumptions are necessary as that of equality between the radial and tangential strains into the minimum section where $Z = 0$. However, it follows that the radial and tangential stresses are equal and the deflector is independent of the radial coordinate (r) for this style. With these assumptions, the equilibrium equations and the plasticity criterion, it is shown that:

$$\frac{d\sigma_{rr}}{dr} = -\frac{\sigma_{eq}}{\rho} \quad (4)$$

With (r) is the radius of curvature of isostatic lines, where they intercept the plane $Z = 0$.

Bridgman (1994) was assumed that isostatic lines can be treated as circles that intersect at right angles of the notch which is the ring [Cayzac, Saï, and Laiarindrasana (2013)].

The radius (r) of curvature is given by (eq 5):

$$\rho = \frac{a^2 + 2aR - r^2}{2r} \quad (5)$$

The average axial force $\bar{\sigma}_{ZZ}$ i.e. the load applied to the test piece is given by the following expression (6):

$$\bar{\sigma}_{ZZ} = \sigma_{eq} \left(1 + \frac{2R}{a}\right) \ln\left(1 + \frac{a}{2R}\right) \quad (6)$$

The ratio of maximum stress triaxiality is on the axis of the specimen such as (7):

$$\frac{\sigma_m}{\sigma_{eq}} = \frac{1}{3} + \ln\left(1 + \frac{a}{2R}\right) \quad (7)$$

Thus as shown in Fig. 3 the stress profile is a parabola, with a maximum at the center of the specimen. The axial stress will be proportionately higher than the

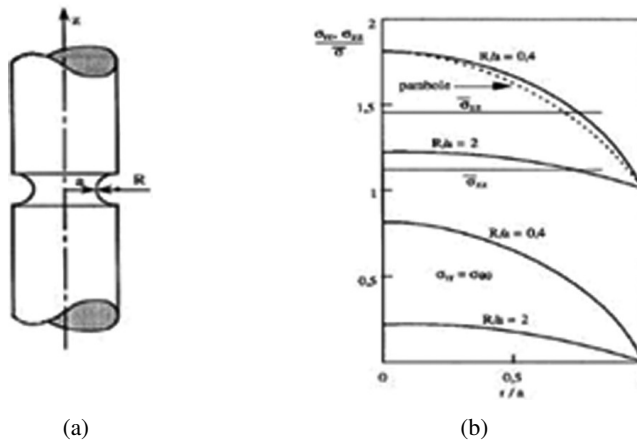


Figure 3: (a) Schematic of the specimen AE, (b) Distribution of the axial stress, radial and tangential as calculated by Bridgman.

radius of curvature R will be low. Choice has occurred in this work on AE specimen four different radii of curvature in order to study the influence of the rate of stress triaxiality on the behavior of “damage” material.

The four radii studied are $R = 80$ mm (AE80), 10 mm (AE10), 4 mm (E4) and 2 mm (AE2) respectively. The geometries of the specimen are such that the total length is 66 mm, the diameter of the barrel is 10 mm, and the bottom of notch diameter is 5 mm (Fig. 4).

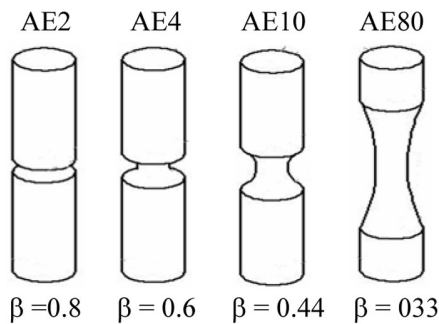


Figure 4: AE specimen geometry.

The studied geometries by notched symmetry (axisymmetric), only quarter of the specimen is meshed with reduced quadratic axisymmetric element integration. Thus, because of the symmetry it is possible to mesh the quarter length to represent the entire structure as shown in Fig. 5. In the indented area, the mesh is finished, unlike

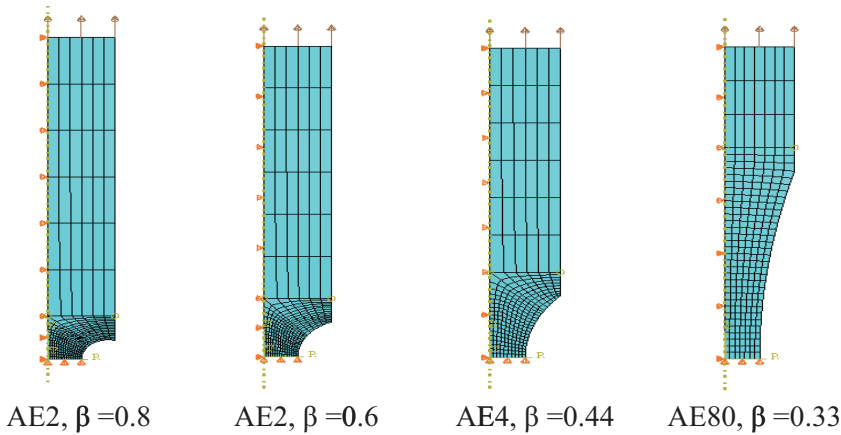


Figure 5: Mesh of the quarter specimens test.

the smooth area where it is coarser.

The tests on the specimen were made in AE with imposed displacement. Numerically it is not possible to return to such a condition directly in the calculation load. At first, the longitudinal displacement of the test was measured at a test speed of variable diameter reduction.

3 Results and discussion

Fig 6 (a, b, c and d) shows a simulation of the stress-strain curve taken at the critical point of the specimen to the four radii obtained ($\beta = 0.33$ for AE80, $\beta = 0.44$ for AE10, $\beta = 0.6$ for AE4 and $\beta = 0.8$ for AE2) for tensile tests at four different speeds (0.2, 0.6, 1 and 1.4 mm/s). We note that with the same displacement, the stress is higher when the radius of curvature is smaller. In the test AE80, there is an increase in the maximum stress and a diameter reduction. In contrast, between AE4, AE2 and AE10, no difference in the maximum stress is observed, while a decrease diameter is obtained. So it seems that beyond a radius value limit, the maximum stress is “saturated”. Only analyzes for low speed are presented, knowing that the same interpretation can be made for higher speeds. On the general appearance of the curves, two interesting results are worth mentioning. The first is the presence of a tow hook at the maximum end; this hook may indicate either a structural effect, or a softening of the material. In the case of a structural effect, the traction hook indicates the rapid formation of the constriction which supports the majority of the stress and elongation.

It then reflects softening attributed to the formation and growth of cavities formed at the location of the deformation in the notched area. The second interesting point

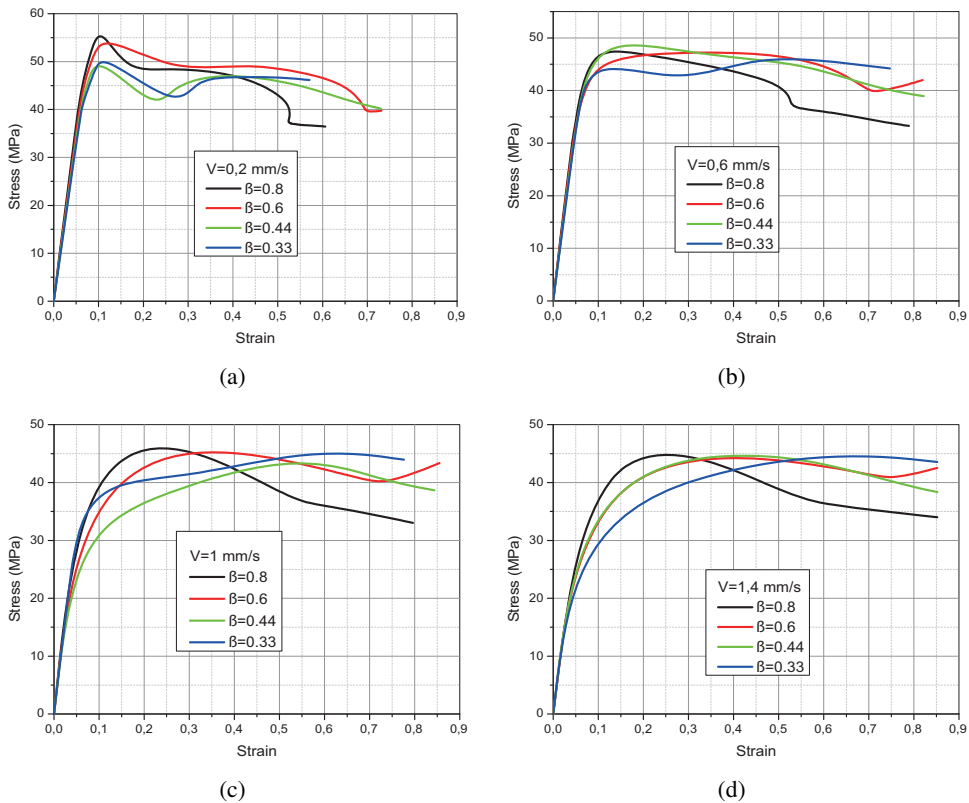


Figure 6: Effect of triaxiality on the constitutive law for four speeds sollicitation.

concerns the plastic deformation tray. The load remains almost constant as the diameter reduction and the end of analysis for AE80 is characterized by work hardening. This result indicates a strong plastic flow associated with orientation and sliding strings. Finally, the fibrils are highly stretched, and then they create additional resistance.

Fig. 7(a, b, c, d) illustrates stress vs strain curves at different strain rate ($v = 0.2$, $v = 0.6$, $v = 1$ and $v = 1.4$ mm/s) with the variation of ($\beta = 0.8$, $\beta = 0.6$, $\beta = 0.44$ and $\beta = 0.33$), in this figure we can see the influence of the rate of stress triaxiality β on the mechanical properties of the material studied and we can pronounce that the same shape of the curves is observed. We note that the presence of the hook still in the smallest speed. In the test $v = 0.2$ mm/s et $\beta = 0.8$ there is an increase in the maximum stress. In contrast, between $v = 1$ mm/s and $v = 1.4$ mm/s any difference in the maximum stress is observed, while a reduction in diameter is obtained.

Fig. 8 (a, b, c, d) shows the evolution of the deformation according to the thickness

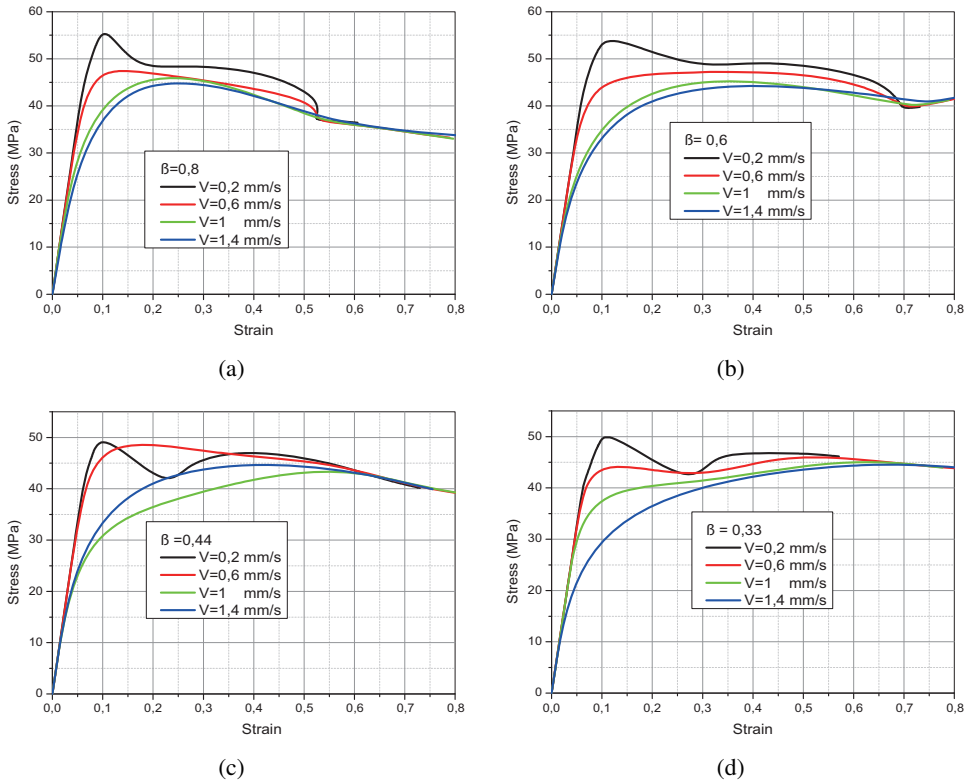


Figure 7: Effect of the strain rate.

of the specimen (diametral position) for each radius of curvature R , indicating the influence of strain rate on this evolution. It is noted from this representation that the deformation progress from the heart to the outside position, whatever the strain rate and is important for the high strain rate, but for the case when $R = 2$ mm and the speed $V = 1.4$ mm/s, the deformation is significant which causes quick failure of the specimen. It is deduced from this study that the notch bottom is the most critical position. In particular for the curvature radius $R = 2$ mm and the strain rate $V = 1.4$ mm/s.

Fig. 9 represents the levels equivalent stresses (Von Mises) in function of the variation of the notch radius at different speeds. Firstly, these stresses are concentrated in the bottom of the notch, the concentration decreases in the way from the notch is noted on the other hand, it increases with increasing radius of the notch, and that the distribution of these stresses is not homogeneous on the side closest to the fault is subjected to relatively low stress amplitude. The largest stresses are located at the bottom of the notch, the amplitude decreases gradually from this zone. If the

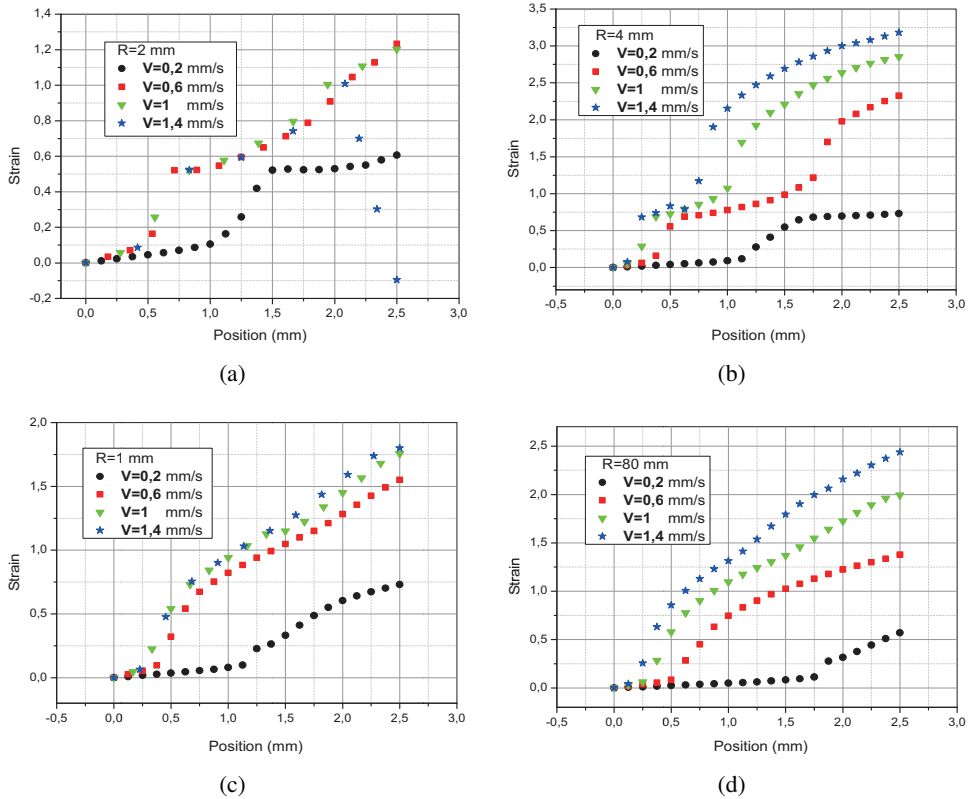


Figure 8: Evolution of strain versus specimen thickness.

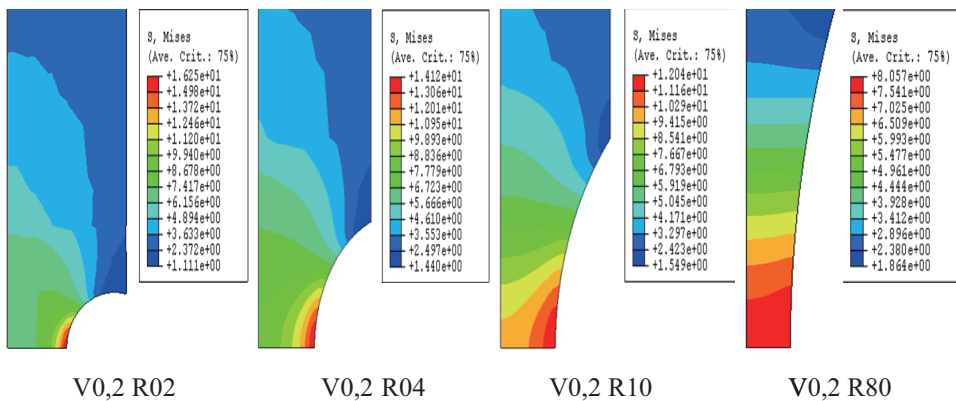


Figure 9: Stress distribution for different notch root radius of curvature.

stress exceeds the elastic limit of the material, a plastic region in the vicinity of the bottom of notch appears.

We also note that the damage was located in the area of the smallest radius of the specimen. It thus appears that these test pieces are adapted to highlight damaged by cavitations. For higher speeds, the effect of speed on the diametric reduction is demonstrated (reduced diametric reduction with increase in strain rate of the specimen).

4 Conclusion

Gurson-Tvergaard-Needleman model usually used for metallic materials [Tvergaard and Needleman (1984); Leblond, Perrin, and Devaux (1995)] has been used here to model the damage behavior of PVC. The damage in this model is described as being due to the growth of cavities, represented by parameters. The importance of damage during deformation has led us to use the GTN model that allows the coupling of the constitutive law with the effect of damage. The model was used to account for all mechanical results and determine a related failure mode and failure by crazing approach, a critical criterion in fibril elongation at low rate and triaxiality criterion coalescence of cavities rates triaxiality high. On behavior, effective plastic strain rate is described by the law of Norton. Hardening is considered isotropic, consists of a constant threshold elastoplastic behavior, describing a saturation deformation crystalline and amorphous phases, and an increase of the rigidity of elongated channels (work hardening). The latter describes exponential for large deformations, the fibril orientation and crystalline phases. The damage is taken into account by adjusting the parameters of the model on the evolution of volumetric strain, and on the draw hook reflecting the softening load due to the strong growth of cavities.

References

- ASTM D638.** (2010): *Standard test method for tensile properties of plastics*, West Conshohocken, PA, USA: American Society for Testing and Materials.
- Bahadur, S.** (1973): Strain hardening equation and the prediction of tensile strength of rolled polymers. *Poly Eng Science*, vol. 13, no. 4, pp. 266–272.
- Bendouba, M.; Djebli, A.; Aid A.; Benseddiq, N.; Benguediab, M.** (2015): Time-Dependent J-Integral Solution for Semi-elliptical 3 Surface Crack in HDPE. *CMC: Computers, Materials & Continua*, vol. 33, no. 2, pp. 111–154.
- Boisot, G.; Laiarinandrasana, L.; Besson, J.; Fond, C.; Hochstetter, G.** (2011): Experimental investigations and modeling of volume change induced by void growth in polyamide. *Int J Solids Struct*, vol. 48, no. 19, pp. 2642–2654.

Bridgman, P. W. (1944): The stress distribution at neck of the tension specimen. *Transactions ASM*, vol 32, pp. 553–574.

Castagnet, S.; Deburck, Y. (2007): Relative influence of microstructure and macroscopic triaxiality on cavitation damage in a semi-crystalline polymer. *Mater Sci Eng A*, vol. 448, no. 1, pp. 56–66.

Cayzac, H. A.; Sai, K.; Laiarinandrasana, L. (2013): Damage based constitutive relationships in semi-crystalline polymer by using multi-mechanisms model. *Int J Plast*, vol. 51, pp. 47–64.

Dahoun, A. (1992): plastic behavior and semi crystalline polymers deformation textures in uniaxial tension and simple shear, PhD Thesis, Ecole des Mines de Nancy, France.

Dong, L.; Atluri, S. N. (2012a): SGBEM (Using Non-hyper-singular Traction BIE), and super elements, for non-collinear fatigue-growth analyses of cracks in stiffened panels with composite-patch repairs. *CMES: Computer Modeling in Engineering & Sciences*, vol. 89, no. 5, pp. 417–458.

Dong, L.; Atluri, S. N. (2012b): SGBEM Voronoi Cells (SVCs), with embedded arbitrary shaped inclusions, voids, and/or cracks, for micromechanical modeling of heterogeneous materials. *CMC: Computers, Materials & Continua*, vol. 33, no. 2, pp. 111–154.

Eyring, H. (1936): Viscosity, Plasticity and Diffusion as Examples of Absolute Reaction Rates. *J Chem Phys*, vol. 4, pp. 283.

G'sell, C.; Jonas, J. J. (1981): Yield and transient effects during the plastic deformation of solid polymers. *J Mat Sci.*, vol. 16, no. 7, pp. 1956–1974.

G'sell, C.; Dahoun, A. (1994): Evolution of microstructure in semi-crystalline polymers under large plastic deformation, *Mat sci Eng.*, vol. 175, no. 1–2, pp. 183–199.

Gurson, A. L. (1977): Continuum Theory of Ductile Rupture by Void Nucleation and Growth: Path I-Yield Function and Flow Rules for Porous Ductile Media. ASME Transaction. *J Eng Mat Tech.*, vol. 99, pp. 2–17.

Kichenin, J. (1992): Thermomechanical behavior of polyethylene-Application to gas structures, PhD Thesis, Ecole Polytechnique, France.

Laiarinandrasana, L.; Besson, J.; Lafarge, M.; Hochstetter, G. (2009): Temperature dependent mechanical behaviour of PVDF: experiments and numerical modelling. *Int J Plast*, vol. 25, no. 7, pp. 1301–1324.

Laiarinandrasana, L.; Morgeneyer, T. F.; Proudhon, H.; N'guyen, F.; Maire, E. (2012): Effect of multiaxial stress state on morphology and spatial distribu-

tion of voids in deformed semi crystalline polymer assessed by X-ray tomography. *Macromolecules*, vol. 45, no. 11, pp. 4658–4668.

Lamloumi, R.; Hassini, L.; Lecomte-Nana, G. L.; Elcafsi M. A.; Smith, D. (2014): Modeling of Hydro-Viscoelastic State of Deformable and Saturated Product During Convective Drying. *CMC: Computers, Materials & Continua*, vol. 43, no. 3, pp. 137–151,

Leblond, J. B.; Perrin, G.; Devaux, J. (1995): An improved Gurson-type model for hardenable ductile metals. *Europ J Mech Solids*, vol. 14, no. 4, pp. 499–527.

Meddah, H. M.; Selini, N.; Benguediab, M.; Bouziane, M.; Belhamiani, M. (2009): Analysis of the polypropylene mechanical behaviour response: Experiments and numerical modeling. *Mat Des.*, vol. 30, no. 10, pp. 4192–4199.

Ognedal, A. S.; Clausen, A. H.; Dahlen, A.; Hopperstad, O. S. (2014a): Behavior of PVC and HDPE under highly triaxial stress states: An experimental and numerical study. *Mech Mat.*, vol. 72, pp. 94–108.

Ognedal, A. S.; Clausen, A.; Berstad, T.; Seelig, T.; Hopperstad, O. S. (2014b): Void Nucleation and Growth PVC – An Experimental and Numerical Study. *Int J Solids Struct*, vol. 51, no. 7–8, pp. 1494–1506.

Ouakka, A.; Dang Van, K.; Gueugnaut, D.; Blouet, P. (1997): *An assessment of the defects damages in polyethylene Gaz pipes.* In 10th Int conf on deformation yield and fracture of polymers Cambridge. The Chameleon Press Ltd. pp. 557–560.

Paquin, A.; Berveiller, M. (1996): Various ways for the micromechanical modeling of the behavior elastoviscoplastic of semicrystalline polymers. *Annual conference of the French Group of Rheology*, vol. 15, pp. 23–28.

Polanco-Loria, M.; Clausen, A.H.; Berstad, T.; Hopperstad, O.S. (2010): Constitutive model for thermoplastics with structural applications. *Int J Impact Eng.*, vol. 37, no. 12, pp. 1207–1219.

Santos, P. G., Carbajo, J., Godinho L., Ramis, J. (2014): Sound Propagation Analysis on Sonic Crystal Elastic Structures using the Method of Fundamental Solutions (MFS). *CMC: Computers, Materials and Continua*, vol. 43, no. 2, pp. 109–136.

Tvergaard, V.; Needleman, A. (1984): Analysis of the Cup-Cone Fracture in a Round Tensile Bar. *Acta Metallurgica*, vol. 32, no. 1, pp. 157–169.

Wu, P.D.; Van Ver Giessen, E. (1993): On improved network models for rubber elasticity ad their application to orientation hardening in glassy polymers. *J Mech Phys Solids*, vol. 41, no. 3, pp. 427–456.

